Surface micropatterning for the formation of an in vitro functional endothelial model for cell-based biosensors

Zhor Khadir, Victor Schmidt, Kevin Chabot, Jean-François Bryche, Ulrike Froehlich, Julien Moreau, Michael Canva, Paul Charette, Michel Grandbois

Surface micropatterning for the formation of an *in vitro* functional endothelial model for cell-based biosensors

Zhor Khadir [a,b,c,d], Victor Schmidt [e], Kevin Chabot [a,b,c], Jean-François Bryche [a,b], Ulrike Froehlich [c], Julien Moreau [d], Michael Canva [a,b,d], Paul Charette [a,b,c], Michel Grandbois [a,b,c,*]

[a] *Laboratoire Nanotechnologies Nanosystèmes (LN2 – IRL 3463) - CNRS, Université de Sherbrooke, Québec, J1KOA5, Canada*
[b] *Institut Interdisciplinaire d'Innovation Technologique (3IT), Université de Sherbrooke, Québec, J1KOA5, Canada*
[c] *Département de Pharmacologie et Physiologie, Université de Sherbrooke, Québec, J1H5H3, Canada*
[d] *Laboratoire Charles Fabry, Institut d'Optique Graduate School, CNRS, Université; Paris Saclay, Palaiseau, 91120, France*
[e] *Mila, Université de Montréal, Québec, H2S 3H1 Canada*

ARTICLE INFO

Keywords:
Surface micropatterning
Endothelium model
Cell-based biosensing
Cell response
Surface plasmon resonance imaging

ABSTRACT

Label-free biosensing, such as with surface plasmon resonance (SPR), is a highly efficient method for monitoring the responses of living cells exposed to pharmacological agents and biochemical stimuli *in vitro*. Conventional cell culture protocols used in cell-based biosensing generally provide little direct control over cell morphologies and phenotypes. Surface micropatterning techniques have been exploited for the controlled immobilization and establishment of well-defined cell morphologies and phenotypes. In this article, surface adhesion micropatterns are used to control the adhesion of endothelial cells within adjacent hexagonal microstructures to promote the emergence of a well-controlled and standardized cell layer phenotype onto SPR sensor surfaces. We show that the formation of cell-cell junctions can be controlled by tuning the inter-cellular spacing in groups of 3 neighbouring cells. Fluorescence microscopy was used to confirm the formation of vascular endothelium cadherin junctions, a structural marker of a functional endothelium. In order to confirm the functionality of the proposed model, the response to thrombin, a modulator of endothelium integrity, was monitored by surface plasmon resonance imaging (SPRI). Experiments demonstrate the potential of the proposed model as a primary biological signal transducer for SPRI-based analysis, with potential applications in cell biology, pharmacology and diagnostic.

1. Introduction

The natural assembly of biological cell layers such as the endothelia and epithelia ubiquitously found in organs and tissues strongly rely on spatially regulated cell-cell and cell-substrate interactions to produce well-defined functional phenotypes. The vascular endothelium is a highly specialized cell monolayer lining the inner part of blood vessels. Depending on its localization in the vasculature, the endothelium exhibits important structural and functional heterogeneity that support various haemostatic functions (Aird, 2012). Of particular importance is its role as a semi-permeable barrier regulating molecular, macromolecular and cellular exchanges between the blood and the underlying tissues (Mehta and Malik, 2006; Vandenbroucke et al., 2008) and its response to mechanical signals associated to blood pressure and flow (Van Hinsbergh, 2001; Wallez and Huber, 2008). The structural and mechanical integrity of the vascular endothelium as a cell layer involves intercellular interactions mediated by transmembrane proteins such as vascular endothelial (VE)-cadherins (Reglero-Real et al., 2016) and adhesion to the extracellular matrix, which is mainly supported by dense clusters of integrins called focal adhesion points (Zaidel-Bar et al., 2007).

Upon reaching confluence, cultured endothelial cells (ECs) *in vitro* adopt cell monolayer organizations presenting a similar morphological appearance and differentiated functional phenotype to those observed *in vivo* (Gospodarowicz et al., 1976, 1978; Vlodavsky et al., 1979; Birdwell et al., 1978). As such, they have been used as *in vitro* models in many studies (L' Heureux et al., 1998). Since *in vivo* cells are sensitive to their microenvironment due to boundary conditions established by the extra-cellular matrix (ECM), neighbouring cells and blood flow, they are subject to structural, molecular and mechanical cues for their functional

* Corresponding author. Département de Pharmacologie et Physiologie, Université de Sherbrooke, Canada.
E-mail address: Michel.Grandbois@Usherbrooke.ca (M. Grandbois).

https://doi.org/10.1016/j.bios.2022.114481
Received 13 December 2021; Received in revised form 1 June 2022; Accepted 10 June 2022

niche. However, some of this information is lost in conventional culture conditions *in vitro*, making it challenging to produce endothelium models presenting well-controlled morphological and functional features. Many studies have demonstrated that micropatterning techniques are effective tools for providing structural *in vivo* geometrical cues that lead to the establishment of well-defined structural phenotypes (Th é ry, 2010; Tseng et al., 2012; Huang et al., 2017).

Whitesides's group was among the first to develop micropatterning protocols using surface chemistry and microcontact printing to control individual cell adhesion on gold substrates. They showed that cell shape and confinement size dictate whether individual cells grow or die when adhered to a surface (Chen et al., 1997). Specific surface chemistries have been exploited depending on the type of substrate (silanization for glass (Mrksich and Whitesides, 1996) or thiol bonds for gold (Ulman, 1996)) and have enabled the creation of adhesive and non-adhesive regions on substrates to promote or prevent cell adhesion (Mrksich et al., 1997). Théry's group was able to induce well-defined cell cytoskeleton organization in individual cells together with the predictable formation of focal adhesion complexes according to the geometry of a micropatterned substrate (Th é ry et al., 2006). Several other studies have shown that, by controlling the cell shape, it is possible to influence specific aspects of cell functional phenotype such as: growth, apoptosis, motility, polarity, division and differentiation across a population of individual cells (Th é ry et al., 2006; Jeon et al., 2014; Parker et al., 2002; Th é ry et al., 2005; Versaevel et al., 2012; Chen et al., 1998).

Various imaging and analysis techniques (Dincer et al., 2019) have been used to study the functional and phenotypic behaviour of cells as individual objects or as monolayers, adhering to different types of substrates, either unstructured or micropatterned. These techniques can be broadly separated into two main categories: (1) fluorescence techniques using specific molecular fluorescent labels (Toomre and Bewersdorf, 2010) and (2) label-free techniques (Fang, 2011). Label-free techniques provide non-invasive analytical readouts in real-time that are useful in many instances, especially when studying cellular mechanisms that involve a significant reorganization of the cell intracellular content or for which specific markers are not available. As demonstrated by our group and others, among label-free techniques used for cell-based studies, SPRI is a particularly sensitive and versatile method for the quantification of biomolecular interactions (Kodoyianni, 2011), cell-substrate interactions (Bockov á et al., 2019) and individual cell responses to biochemical stimuli (S ö llradl et al., 2018a; S ö llradl et al., 2018b; Yanase et al., 2014).

In this work, we controlled the adhesion and self-assembly of ECs (EAhy926) on biochemically micropatterned gold surfaces. Individual cells were attached to hexagonal spots in groups of three to form a basic unit, with a view to form a functional endothelium model for use in *in vitro* label-free biosensing. This three-cell assembly enabled us to study the effect of confinement of individual cells and the effect of spacing between cells on the formation of cell/cell junctions. Fluorescent labelling of the VE-cadherin junctions between cells confirmed the emergence of a structural endothelium phenotype. In addition, the functionality of the proposed model for use as a cell-based signal transducer was assessed by SPRI following stimulation by thrombin, a well-established method for modulating endothelium integrity.

2. Experimental section

2.1. Gold thin film deposition on glass substrates

The glass substrates used in this study were square coverslips of 22 mm on a side (Fisherbrand). They were cleaned using acetone, isopropanol (IPA) and deionized water, each for 5 min. The glass substrates were put under vacuum (386×10^{-7} Pa) for deposition of a 3 nm titanium adhesion layer followed by a 30 nm gold layer by evaporation.

2.2. Cleaning of gold surfaces

The gold-covered substrates were exposed to oxygen plasma for 10 min at 150 W and 700 mTorr (93.3 Pa). Then, they were cleaned for 10 min in a boiling solution at 70 °C consisting of hydrogen peroxide solution H_2O_2 and deionized water in 1:3 ratio. After washing with deionized water, the substrates were left in 99% pure ethanol for 1 h.

2.3. Passivation of gold surfaces

To passivate the gold surfaces, the freshly cleaned substrates were immersed for 1 h in a 0.5 mM solution of HS-C11-EG6-OH (PEG-SH, Prochimia) in 99% pure ethanol. The passivated substrates were then dried under a stream of nitrogen.

2.4. Micropatterning using deep-UV illumination

Chrome photomasks (PHOTOMASK PORTAL (We Help You Make Masks)) were cleaned with 95% ethanol to remove inorganic residues and dried with a stream of nitrogen. To make the chrome surfaces hydrophilic, the masks were exposed to deep-UV (DUV) light ($\lambda = 184.9$ nm and 253.7 nm, UVO Cleaner model 342-220) for 5 min. A 3 µl drop of deionized water was then deposited on the chrome side of the masks for contact with the pegylated gold-covered side of the substrates. The mask/substrate "stacks" were then exposed to DUV light with the quartz side facing the lamp for 5 min (exposure dose of 900 J/m^2) for spatially selective photodegradation of the surface passivation chemistry. After DUV exposure, a deionized water droplet was used to aide in releasing the substrates from the masks. After drying the substrates with a stream of nitrogen, they were stored in a sample container under vacuum for 3 weeks or more at room temperature.

2.5. Functionalization of the gold surfaces

Before adding cells, the substrates were rinsed for 1 h in pure ethanol to remove molecules photodegraded by the DUV light. After drying, the substrates were incubated with cell adhesion promoters: either 500 µl of 5 µg/ml fibronectin (F0895 Sigma-Aldrich) for 1 h or 200 µl of a mix of fibronectin, collagen and albumin (Athena Enzyme Systems 0407) for 5 min. The incubation times were determined from adsorption kinetics measured by SPR as shown in Fig. 1b. The objective was to maximize adhesion promoter density within the micropatterned areas (photodegraded surface chemistry) while minimizing non-specific adhesion to pegylated areas.

2.6. Cell culture

Immortalized EAhy926 cells (human umbilical vein cell line) were cultured in Dulbecco's Modified eagle's medium supplemented with 10% temperature inactivated foetal bovine serum (FBS) and 60 U/ml penicillin in tissue culture Petri dishes (100 mm diameter). Cells were cultured in 5% CO_2 in an incubator at 37 °C for 3 days until reaching 80–90% confluence. Cells were then trypsined (EDTA 0.25%) and resuspended in 0% FBS. Cells were counted using an automated cell counter kit (MOXI Z). Cells at the desired initial density were seeded onto the functionalized micropatterned substrates in a 35 mm diameter Petri dish. After 2 h of initial adhesion, cells could be fixed to count the number of cells per microstructure as shown in Fig. 2. For studies of cell/cell junction formation, the culture medium containing 10% FBS was replaced with a culture medium containing 0% FBS and 10 µM HEPES. Cells were left to adhere on the micropatterned substrates for 24 h in the incubator.

When imaging cells adhering to the gold substrates using SPRI microscopy, the cells were stimulated by the injection of thrombin (from human plasma T6884 – Sigma-Aldrich). For control experiments, cells were stimulated using RWJ 56110 (Tocris), a selective protease-

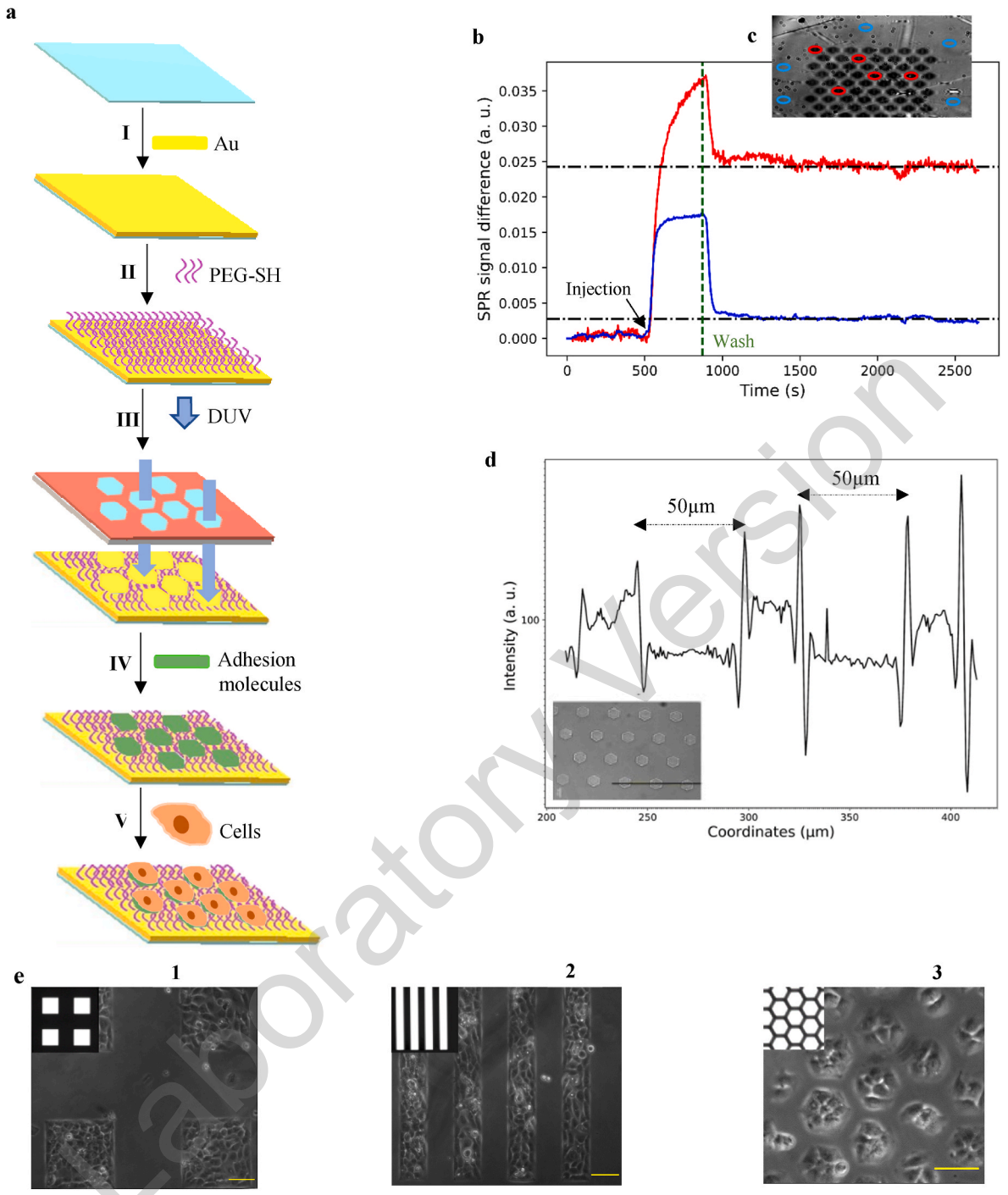

Fig. 1. Spatial patterning of endothelial cell adhesion using DUV micropatterning. a, Micropatterning protocol. I: gold deposition and cleaning, II: Passivation with PEG-SH, III: DUV illumination through a photomask, IV: functionalization with adhesion promoters, V: cell culturing. **b,** SPR kinetics of adhesion promoter deposition inside and outside the DUV illuminated areas of the micropatterned gold surface during step IV: mean intensity of 5 ROIs in the passivated (blue circles) and non-passivated (red circles) areas. The arrow indicates adhesion promoter injection. **c,** SPR image of the gold surface after exposure to DUV illumination through a micropatterned chromed mask **d**, Bright field intensity line profile of hexagons (diameter: 35 µm; spacing: 50 µm) with adhesion promoters labelled with Coomassie-blue at step IV after rinsing as shown in the bright field image of **inset (d)**. **e,** respectively from left to right: Bright field images of fixed endothelial cells (EAhy926) constrained in: **1-** squared adhesion area (the inset shows a bright field image of squares of 250 µm on a side separated by 250 µm in the chromium mask); **2**- lines of 100 µm thickness with a spacing of 100 µm. **3**- Hexagonal array of hexagons of 100 µm diameter with a spacing of 25 µm. (scale bars = 100 µm).

activated receptor-1 (PAR1) antagonist.

2.7. Cell junction and nucleus labelling

Micropatterned substrates with adhered cells were incubated for 1 h in warm L-15 at 37 °C. They were then transferred to a 35 mm Petri dish and incubated in a solution of Fluorescein isothiocyanate (FITC) mouse anti-human antibody for CD144 (BD Pharmingen) at a ratio 1:10 in L-15 for 30 min at 37 °C. After washing with PBS, cells were fixed with 2% PFA/PBS for 10 min at 37 °C. Substrates were then washed 3 times with PBS. The excitation wavelength for the dye is 488 nm with an emission at 520 nm.

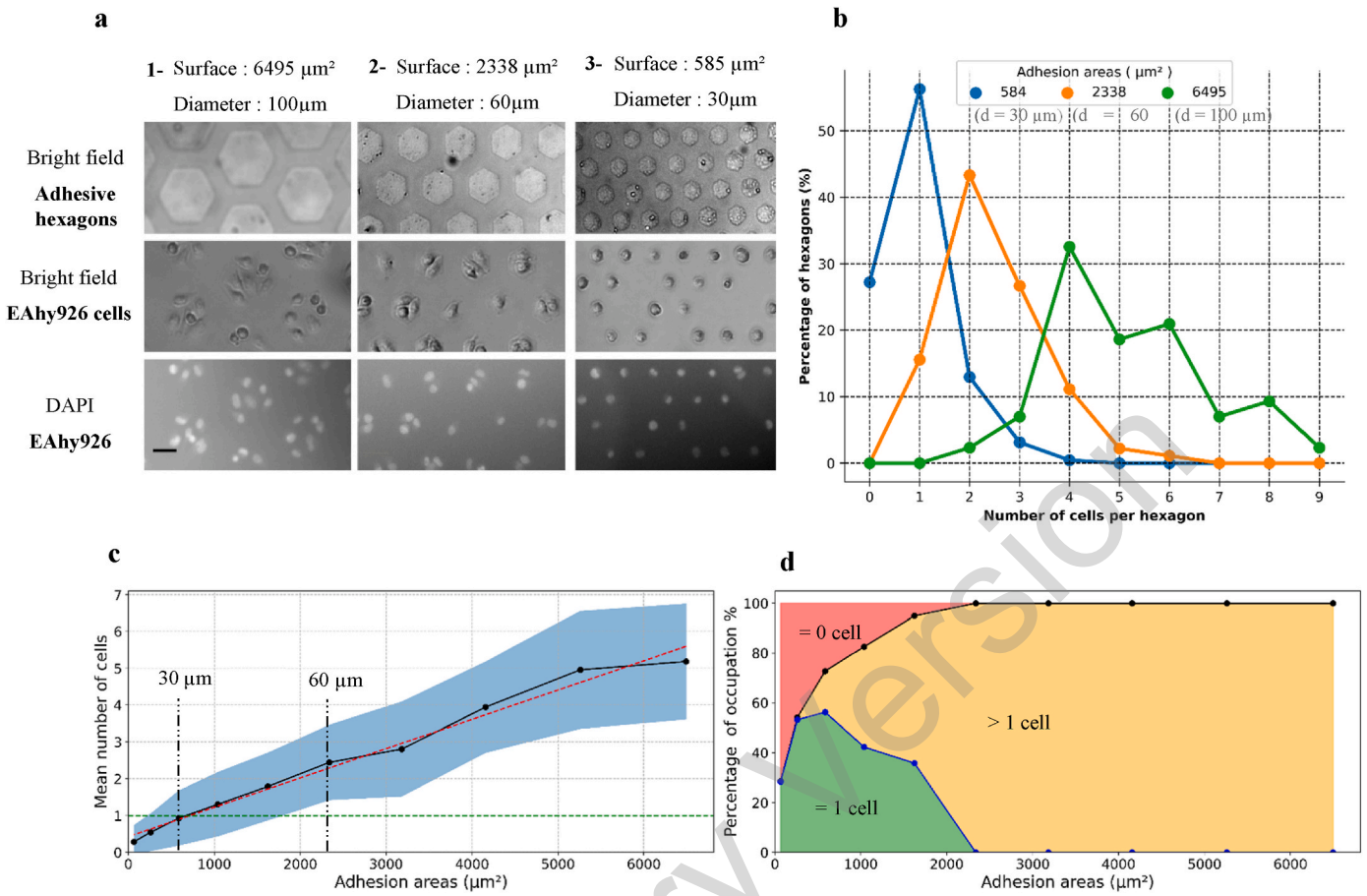

Fig. 2. Confinement of individual endothelial cells in hexagonal microstructures as a function of diameter. a, Bright-field images of Mix-FN coated hexagonal microstructures labelled with Coomassie blue (**top row**) of different surface areas: 6495 µm^2 (**1**), 2338 µm^2 (**2**) and 584 µm^2 (**3**) with a spacing of 25 µm. After 2 h of adhesion, EAhy926 cells adhering in microstructures were fixed (with their bright-field images shown in the **middle row**) and their nuclei were stained with DAPI (with the fluorescence images shown in the **bottom row**). (Scale bar = 50 µm) **b,** Distribution of the number of cells per hexagon as a function of the 3 surface areas shown in (**a**). **c,** Distribution of the mean number of cells per microstructures as function of their adhesion areas. The mean number of cells for each diameter from 100 µm to 10 µm in steps of 10 µm is plotted in the graph. The standard deviation for all diameters is represented by the blue filled area. The red line represents a linear model fit to the data and the 1 cell per hexagon level is shown by the green line. **d,** Percentage occupation of microstructures by cells as a function of surface area. The graph is segmented into 3 regions according to microstructure cell occupation: number of cells greater than 1 (orange), exactly one cell (green), unoccupied (red). The optimal compromise between yield (% occupation) and single cell confinement is reached for surface areas between 406 µm^2 to 585 µm^2 (diameters between 25 µm and 30 µm).

After fixation of cells, samples were incubated in 1 µg/ml solution of 4′,6-diamidino-2-phénylindole (DAPI) in PBS for 15 min at 37 °C in the dark. After removing the staining solution, substrates were washed once with PBS before observation with a fluorescence microscope.

2.8. *Imaging instrumentation*

2.8.1. *Fluorescence microscope*

Bright field images of cells and fluorescence images of nuclei for counting the number of cells in the hexagonal microstructures as function of their diameters were acquired using a Zeiss Axiovert 200 inverted fluorescence microscope with a 10 × magnification objective.

Simultaneous acquisition of fluorescence images (VE-cadherin junctions labelled with a FITC mouse anti-human antibody for CD144 and nuclei labelled with DAPI) and bright field images of cells were taken with a Zeiss AxioImager M2 Apotome with a 40 × objective.

2.8.2. *SPR imaging in Kretschmann configuration using a prism*

The prism-based SPR imaging system used for the real time characterization of the adhesion promoter functionalization on the gold surfaces is described in a previous article (S ö llradl et al., 2017). The micropatterned substrates were mounted on a BK7 glass prism and clamped against a fluidic cell. Spectral scanning from 650 nm to 800 nm was done to identify the optimal SPR observation wavelength. Images in transverse electric (TE) and transverse magnetic (TM) polarizations were collected during the experiments at a frame rate of ~3.5 s between images (TM images contain the SPR information while TE images correct for illumination inhomogeneities). Elliptical regions of interests (3 µm × 7 µm) were positioned manually over selected micropattern units in the SPR images as shown in the insert Fig. 1, b.

2.8.3. *SPR microscopy using a high numerical aperture objective*

The high spatial resolution SPR imaging system used in the experiments described below is described in a previous article (S ö llradl et al., 2017). Briefly, light from a fibre pig-tailed 650 nm polarized LED at the entrance of the SPR microscope passes through a beamsplitter and is scanned in the back focal plane of a high numerical aperture objective to adjust the coupling angle to the backside of the substrate. The reflected beam is returned through the objective, passed through the beamsplitter and is recorded by a CMOS camera. A polarizing beamsplitter in front of the camera splits the beam into the two perpendicular polarizations.

2.9. Image processing

2.9.1. Image segmentation

Fluorescence images and bright field images were taken simultaneously with the same microscope. Segmentation of the nuclei and cells in the fluorescence images was carried out using MorpholibJ (Legland et al., 2016), a library for morphological operations in ImageJ. Segmentation of labelled nuclei images allowed counting the number of cells per hexagonal microstructure. The hexagonal micropatterns were also segmented in the bright field images. A set of Python scripts were developed to perform the segmentation and processing using the NumPy (Harris et al., 2020), Matplotlib (Hunter and Matplotlib, 2007), Scikit-learn (Pedregosa et al., 2011) and Scikit-image (Van der Walt et al., 2014) packages.

2.9.2. Analysis of VE-cadherin junction fluorescence images

To study similarities and variations in cell-cell junction morphology, we developed a Python script for the registration of the groups of three hexagonal microstructures in the fluorescence images. The script first extracted the barycentre coordinates of individual groups of 3 nuclei. From the barycentre coordinates, the centre coordinates of the three hexagons were estimated by fitting a rotated equilateral triangle to the centres of mass of the nuclei, assuming a hexagon diameter of 30 μm and centre-to-centre spacings of 3 μm. The registered images could then to combined in an average intensity map to visualize the location and distribution of the junctions. See supplementary data Fig. 4 for the sequence of operations.

2.9.3. Normalization of SPR images

In the experiments, TM polarization SPR images of the groups of 3 cells were acquired every 10 s for 2 h. TM images corresponding to a point in time where cells were stable before stimulation were subtracted from all subsequent images to reference the SPR signals to zero. Regions of interests (ROI, squares of 80 μm on a side) corresponding to isolated groups of 3 EC cells were positioned manually in the images. Mean background values in negative control areas surrounding the group of cells were subtracted from the signal. Mean pixels values over time in the ROI are plotted in Fig. 5.

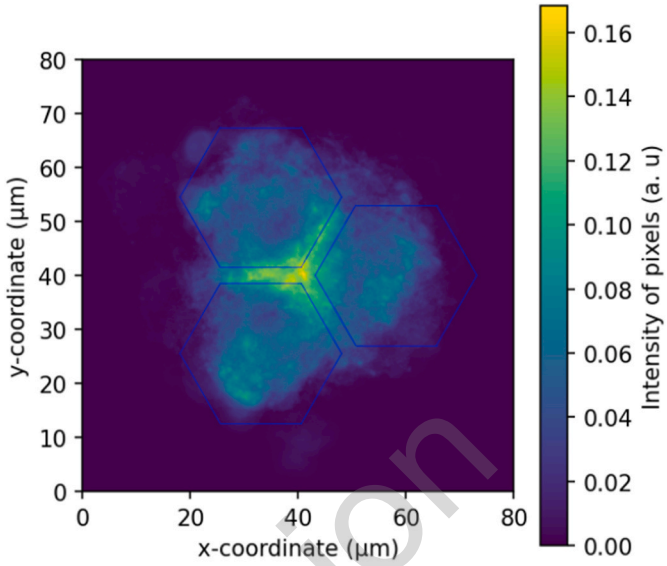

Fig. 4. Micrograph obtained from an average of 40 immuno-fluorescence images (VE-cadherin) of independent 3-cell groups (30 μm diameter hexagons with 3 μm spacing), where the images were aligned automatically (see supplementary data Fig. 4).

3. Results and discussion

In this section, we test the hypothesis that optimization of the adhesion and self-assembly of individual endothelial cells in hexagonal surface micro-patterns can be used to induce the emergence of a normalized functional endothelial cell phenotype *in vitro*. Firstly, we carried out a study of the experimental conditions required for controlled adhesion and confinement of a single endothelial cell per microstructure. Next, spacing between the microstructures was varied to induce, in a controlled manner, the formation of endothelial junctions between the cells. Finally, the functionality of the proposed model was validated using SPRI through the quantification of its response when exposed to thrombin, a well-known modulator of endothelium integrity.

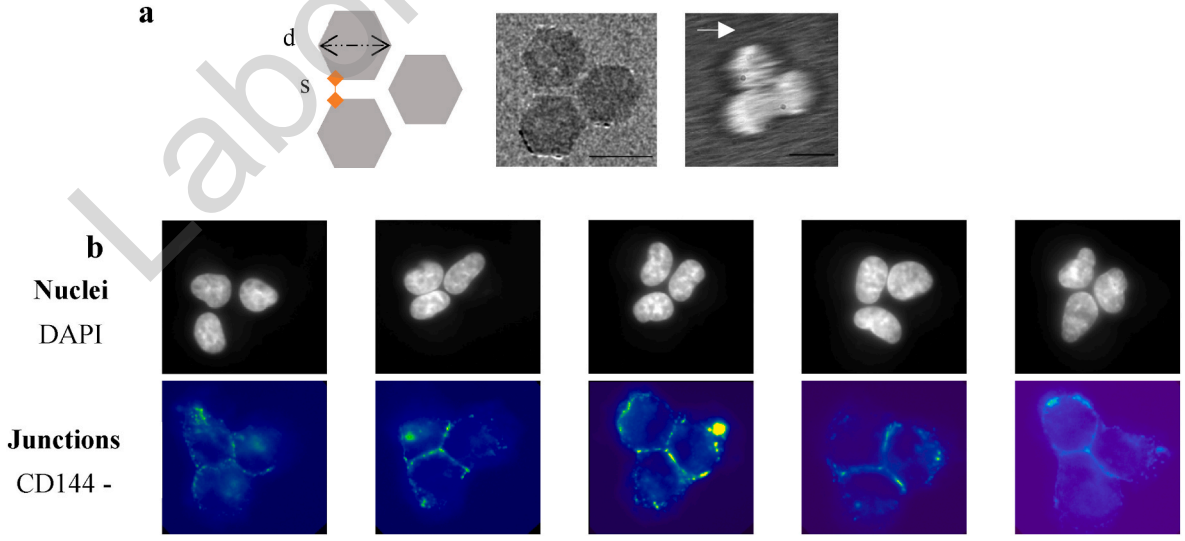

Fig. 3. From individual cells to groups of 3 cells through control of cell-cell connectivity. a, left: Schematic of a group of 3 hexagonal microstructures (diameter d = 30 μm, spacing s = 3 μm). **Middle**: Bright field image of a hexagon group labelled with Coomassie blue. **Right**: SPR image of a hexagon group. The white arrow indicates the surface plasmon propagation direction. Scale bar = 30 μm **b,** Fluorescence micrographs of nuclei labelled with DAPI and VE-cadherin cell-cell junctions labelled using a FITC mouse anti-human antibody targeting CD144, for different groups of 3 hexagons (30 μm diameter, 3 μm spacing). Cells were fixed after 24 h of adhesion.

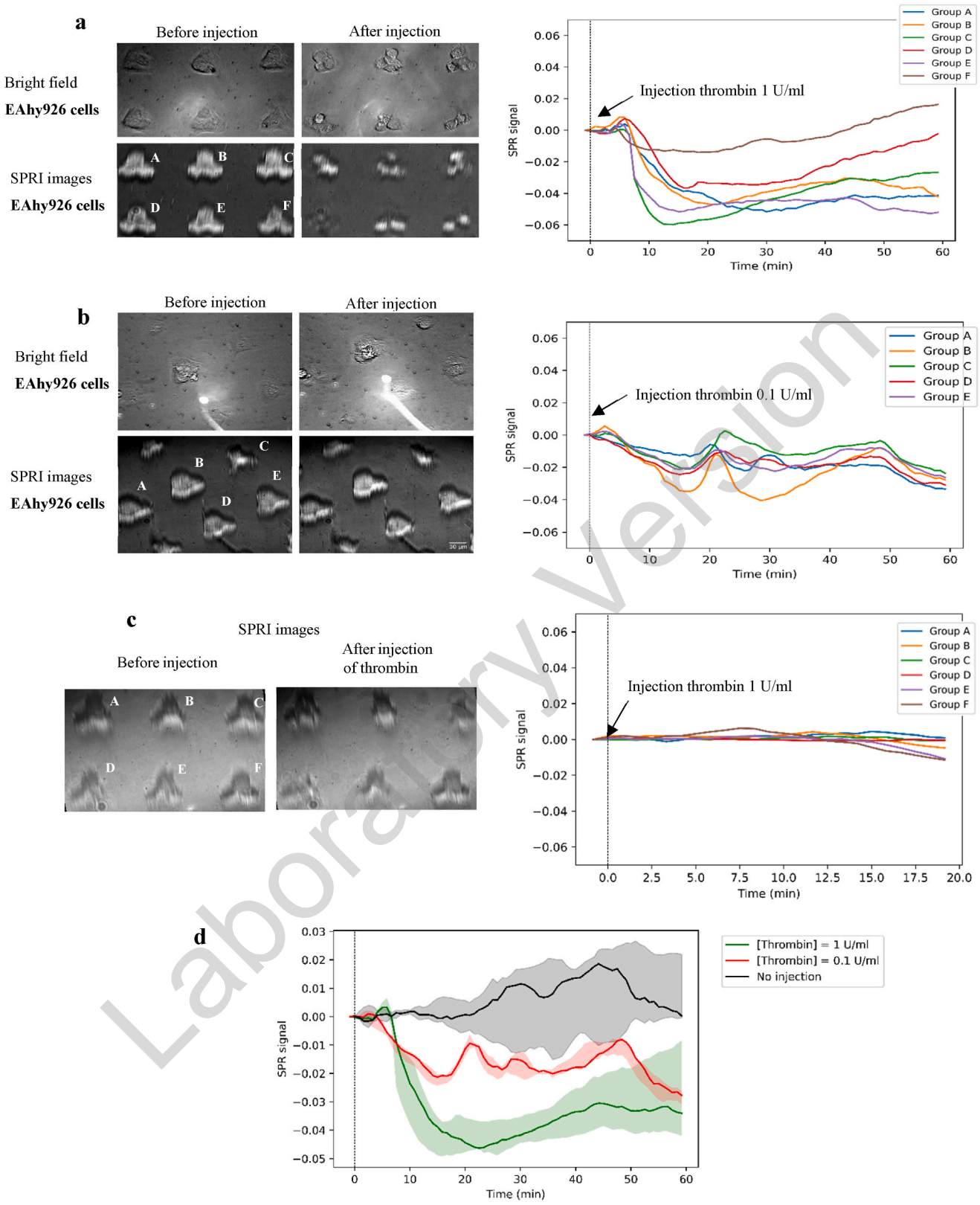

Fig. 5. Examples of time sequences for groups of 3 cells under 3 experimental conditions: graphs **a - c,** show bright field and SPRI images before and after stimulation with thrombin, with corresponding plots over time of normalized pixel intensity across groups of 3 cells in the SPR images for (see experimental section *4.10.4,* all curves are referenced to zero at the time of thrombin injection for better comparison): **a,** 1 U/ml thrombin, **b,** 0.1 U/ml thrombin, **c,** injection of 10 μM RWJ56110 followed by the injection of 1 U/ml thrombin (RWJ56110 is a selective protease-activated receptor-1 (PAR_1) antagonist, SPRI images before injection of the antagonist and after injection of thrombin are shown). **d,** Plots of medians and quartiles (filled area around the curves) after injection of 1 U/ml thrombin (green curve), injection 0.1 U/ml of thrombin (red curve) and control experiment (no thrombin injection, black curve).

3.1. Biomolecular micropatterning protocol

To control the spatial patterning of cell adhesion on the substrate, we developed a micropatterning protocol for gold-covered surfaces passivated with thiolated polyethylene glycol (PEG-SH) using DUV illumination as described above (Fig. 1a). X-ray photoelectron spectroscopy (XPS) characterization of the bare gold surfaces after cleaning (Fig. S1a) showed a main peak (284.8 eV) due to residual contamination carbons (Shchukarev and Korolkov, 2004), while XPS results after passivation with PEG-SH (Fig. S1b) showed two peaks (285 eV and 286.6 eV) due the PEG carbon bonds, confirming successful PEG deposition. DUV lithography with a chrome photomask (hexagonal spots in various sizes and spacings, as well as other shapes such as lines) was used to photodegrade the PEG passivation in areas designated for cell adhesion. Un-patterned control surfaces photodegraded with DUV light appeared homogeneous in optical microscopy images and prevented cell adhesion as expected (inserts Fig. S1b). SPRI was used to confirm the formation of the micropatterns on the substrates (dark areas in Fig. 1c). The photodegraded areas of the surface were then functionalized with a mix of fibronectin, collagen and albumin (Mix-FN) to promote cell adhesion.

In order to validate the surface functionalization, 5 regions of interests were randomly selected for SPRI measurements during functionalization of the passivated (blue) and un-passivated (red) areas. The traces shown in Fig. 1b represent the mean intensity variations over time for the 5 ROIs for each case. Mix-FN was injected (Fig. 1b: black arrow) and incubated for 5 min before rinsing (Fig. 1b: dashed green line). After injection, the SPR signals increased for both area types. After rising for 3 min, the signal corresponding to the PEG-passivated areas (blue curve) returned to the baseline while the signal corresponding to the functionalized areas (red curve) stabilized at a plateau, confirming the selective adhesion of the Mix-FN to the micropatterned areas.

To measure the dimensions of the micropatterned shapes, functionalization molecules labelled with Coomassie-blue were imaged with bright field microscopy (inset Fig. 1d). Line profiles confirmed the dimensions of the patterned shapes (Fig. 1d: hexagons 35 μm in diameter with a spacing of 50 μm). The DUV micropatterning method enable us to pattern a variety of shapes such as square, lines and hexagons at sizes down to few microns in diameter with successful cell adhesion (see Fig. 1e). Hexagons were ultimately selected as the basic unit shape to mimic the *in-vivo* cobblestone-like morphology of ECs in confluent monolayers.

3.2. Cell confinement into hexagonal microstructures

A range of hexagonal microstructures with areas ranging from 65 μm^2 (d = 10 μm) to 6495 μm^2 (d = 100 μm), in increments of 10 μm in diameter, were used to determine the optimum area for the confinement of individual cells. EAhy926 cells were incubated on the micropatterned substrates following the protocol described above. Hexagons were separated by passivated PEG regions of 25 μm width to prevent cell-to-cell contact. After 2 h of incubation, cells were fixed, and their nuclei stained with DAPI to count the number of cells per hexagon. As expected, the distribution in the number of cells per hexagon was found to depend on the surface area of the hexagons. Figs. 2a–1 shows that the largest hexagons (6495 μm^2, d = 100 μm) were occupied by a number of cells that varied between 2 and 9, with a fairly broad distribution (Fig. 2b). For hexagons of 2338 μm^2 (d = 60 μm) (Fig. 2a–), the range in the number of cells per microstructure decreased to 1 to 6 (Fig. 2b). Finally, for 585 μm^2 hexagons (d = 30 μm) (Figs. 2a–3), the range in the number of cells decreased to 0 to 3 (Fig. 2b) with a distribution centred on 1 cell per microstructure.

Fig. 2c shows the distribution of the mean number of cells per microstructures as a function of area (μm^2). A linear fit to the data (red curve) indicates that 713 μm^2 (diameter of 33 μm) is ideal for single cell confinement. The closest available micropatterns size in the mask (30 μm) was thus selected for the confinement of single cells into the microstructures. The graph plotted in Fig. 2d represents the percentage occupation of microstructures by cells as a function of hexagon surface area. The graph is segmented into 3 regions: the orange region corresponds to microstructures occupied by a number of cells greater than 1. The green region corresponds to microstructures occupied by exactly one cell. Finally, the red region represents unoccupied microstructures. These results indicate that the adhesion yield by ECs decreased with hexagon area. The optimal compromise between yield (percentage of occupation) and single cell confinement was reached for hexagons with surface areas between 585 μm^2 to 406 μm^2 (diameters between 25 μm and 30 μm), which is consistent with EAhy926 cells in confluent films *in vitro* (Laposata et al., 1983) (diameters from 25 μm to 35 μm). Note that the probability of obtaining one cell per hexagon also depended on the incubation time, as explained below.

3.3. Optimal cell-cell separation in a 3 cells group for the formation of junctions

The next step in the study was to vary the separation between the hexagons, thus the connectivity between individual ECs, to promote the formation of cell-cell junctions in groups of 3 neighbouring cells (Fig. 3a). Before junction formation can take place, cells can undergo division and proliferation. To inhibit these normal cellular activities, in particular cell division, we optimized key parameters to maximize the likelihood of obtaining 1 cell per hexagon in the groups of 3 neighbouring hexagons (total of 3 cells). These parameters included initial density of cells, growth factor in the cellular medium (foetal bovine serum FBS), as well as two temporal parameters: the time required for cells to occupy the majority of hexagons and the time to form cell-cell junctions. An estimated initial EAhy926 cell density of 500 000 cells/ml was cultured on the micropatterned gold substrates for an initial time of 2 h, in a culture medium with 10% FBS. The culture medium was then changed to discard non-adhered cells and replaced with a fresh medium without FBS. After 24 h in the incubator, cells were fixed and the VE-cadherin junctions and nuclei were labelled with FITC anti human mouse CD144 and DAPI, respectively.

We studied the formation of cell-cell junctions in the groups of 585 μm^2 hexagons, where the separation between hexagons in a group varied from 0 μm to 7 μm, in steps of 1 μm. We observed that the probability of obtaining 1 cell per hexagon was dependant on the inter-hexagon spacing in a group. Indeed, the probability of observing 1 cell per hexagon was highest for spacings between 3 μm and 5 μm (Fig. S2). Furthermore, Fig. S3 shows that cells are in contact for a 3 μm spacing but are clearly separated for a 7 μm spacing. Hence, the range of spacings for which the probability of having one cell per hexagon was highest and which favoured the formation of cell-cell junctions was between 3 μm and 5 μm. We chose to work with the closer configuration (3 μm spacing). Fig. 3b shows 5 different groups of 3 hexagons (30 μm diameter, 3 μm spacing) from two different experiments. The labelling of nuclei with DAPI confirmed that there was exactly 1 cell per hexagon. In addition, VE cadherin junction labelling indicated the formation of Y-shaped cell-cell junctions in the groups.

The visualization of VE-cadherin junctions in the 3 cells groups (Fig. 3b) demonstrated the establishment of a structural phenotype consistent with that of an EC monolayer. Fig. 4 shows the average of 40 fluorescently labelled VE-cadherin junction images taken from separate 3-cell groups (30 μm diameter hexagons with 3 μm spacing), where the images were aligned automatically as described above (see supplementary data Fig. 4). As expected, the image shows that the highest intensities are along the cell-cell junctions, demonstrating a high level of uniformity among the 3 cell groups. The location of the cell-cell junctions corresponds to the pegylated non-adhesive areas between hexagonal microstructures, confirming that cell-cell junctions were formed between cells according to the geometries of the micropatterned substrate. Note that averaging more than a few tens of micrographs did not

significantly improve the quality of this result which was meant to confirm the uniformity of the structural phenotype in the EC 3-cell groups.

3.4. Label-free SPR characterization of the endothelial functionality of the 3 cells groups

Biosensing based on SPR imaging is a sensitive and non-invasive label-free technique for visualizing and quantifying biological objects and measuring living cell response in terms of adhesion and motility (Abadian et al., 2014) in the presence of endotoxins and receptor agonist (Cuerrier et al., 2008; Chabot et al., 2009). To evaluate the functional phenotype of the groups of 3 cells, we quantified their responses to a stimulus using our high-resolution SPRI system. Thrombin, a serine protease that activates the cell protease-activated receptor 1 (PAR_1) constitutively expressed in ECs was used to stimulate the cells (S ö llradl et al., 2018b; S ö llradl et al., 2017). Thrombin signalling in the endothelium results in the activation of intracellular signalling pathways that leads to cell contraction and cell rounding, cytoskeleton remodelling, disruption of cell-cell junctions with disassembly and re-modelling of cell attachments to the substrate (Minami et al., 2004; Opal and van der Poll, 2015). Fig. 5 shows typical responses of distinct groups of cells, acquired in real-time using the SPRI system. Thrombin was injected 30 min after beginning the experiment (t = 0 in the plots) in a temperature-controlled fluidic chamber (T = 37 °C) at 2 concentrations (units/ml): 1 U/ml and 0.1 U/ml. Bright field images were taken at the beginning of the experiments before injection of thrombin and at the end of the experiments. SPRI images are highly sensitive to changes in cell interactions with the surface due to the shallow plasmon mode penetration depth (~200 nm above the surface at visible wavelengths). Note however that the lower spatial resolution along the axis of light propagation in SPRI cannot resolve details inside the cells.

Following the injection of thrombin at 1 U/ml (Fig. 5a), cells responded within 10 min with the SPRI signal rapidly dropping, followed by a recovery trend where the speed of recovery varied from one cell group to another. The first phase of the SPRI signal variations is due to cell contraction and an increase in the intercellular gaps, followed by a recovery phase associated with cell spreading on the surface. The thrombin response is observable in the SPRI images where cells inside the groups of 3 hexagons show less contrast due to loss of cell adhesion from the surface. This is similar to what is observed in a confluent endothelial cell monolayer with a reversible response (Vouret-Craviari et al., 1998). The activation of the PAR_1 receptor by thrombin is well documented and the resulting SPRI images were consistent with the cellular responses obtained from conventional EC monolayers *in vitro* (Chabot et al., 2009; Nobe et al., 2005). The lowest concentration of thrombin (0.1 U/ml, **Fig. 5b**) induced a weak response as seen by the low amplitude variations in the SPRI signal, similar to the control experiment. Indeed, at lower concentrations of thrombin, sub-threshold activation of the receptor is expected thus leading to heterogeneous and unstable responses.

As a control experiment to confirm that the SPRI responses were directly related to the activation of the PAR_1 receptor by thrombin, the cells were exposed to a selective antagonist (RWJ56110) of the PAR_1 receptor prior to the injection of thrombin (Andrade-Gordon et al., 1999) at 1 U/ml (Fig. 5c). No significant SPR signal variation was observed after injection of thrombin for all 6 groups of 3 cells (the antagonist strongly binds to the PAR_1 receptor and prevents its activation by thrombin). This confirmed that the responses observed following the injection of thrombin in Fig. 5a and **b** were indeed due to the activation of the PAR_1 receptor (Zania et al., 2006). Fig. 5d compares the SPR signal responses for concentrations of 1 U/ml and 0.1 U/ml thrombin to a control experiment where no thrombin was injected. To highlight the heterogeneity of cellular responses, medians with their quartiles represented by the filled area around curves were plotted. Taken together, these results demonstrate that a group of 3 ECs exhibits the barrier and functional phenotype of an endothelial layer, consistent with previous studies on EC monolayers *in vitro* (S ö llradl et al., 2018a; S ö llradl et al., 2018b; Chabot et al., 2009).

4. Conclusion

In this work, we demonstrated the fabrication of an *in vitro* model elementary unit consisting of 3 EAhy926 connected cells, a first step toward a more complete EC monolayer model. This was achieved by controlling adhesion and by constraining cells into adjacent hexagonal areas of well-defined size and spacing. To this end, we developed a micropatterning protocol combining surface thiol chemistry and Deep-UV illumination through a photomask for the fabrication of cell adhesion micropatterns on gold surfaces. We identified a range of sizes for which the confinement of a single endothelial cell per hexagonal microstructure could be reliably obtained. By inserting a 3 μm spacing between hexagons, it was possible to induce connectivity between individual cells to establish VE-cadherin junctions, demonstrating a phenotypically relevant endothelial cell monolayer model. Finally, SPRI microscopy was used as a label-free analytical modality to confirm the functional response of the proposed EC model following thrombin stimulation. This work demonstrates that an *in vitro* model of a functional cell layer phenotype, where the adhesion, confinement and connectivity between individual ECs are controlled by substrate micropatterning, can be used as a primary biological signal transducer with surface plasmon resonance imaging. The proposed strategies could be applied to a wide variety of endothelial and epithelial cell types to produce structurally and functionally normalized cell monolayer models for biological studies and biosensor applications.

CRediT authorship contribution statement

Zhor Khadir: Conceptualization, Methodology, Software, Investigation, Visualization, Writing – original draft. **Victor Schmidt:** Software, Investigation, Visualization. **Kevin Chabot:** Data curation. **Jean-François Bryche:** Conceptualization, Methodology. **Ulrike Froehlich:** Methodology, Data curation. **Julien Moreau:** Methodology, Supervision, Writing – review & editing. **Michael Canva:** Supervision, Writing – review & editing. **Paul Charette:** Supervision, Writing – review & editing. **Michel Grandbois:** Supervision, Writing – review & editing.

Declaration of competing interest

The authors declare that they have no known competing financial interests or personal relationships that could have appeared to influence the work reported in this paper.

Acknowledgments

This work was supported financially by the National sciences and engineering research council of Canada (NSERC) Discovery grants of M. Canva, P.G. Charette, and M. Grandbois. Z. Khadir benefited from a Mitacs Globalink scholarship. LN2 is an International Research Laboratory (IRL) funded and co-operated by Université de Sherbrooke (UdeS), Centre National de la Recherche Scientifique (CNRS), Ecole Centrale Lyon (ECL), Institut National des Sciences Appliquées de Lyon (INSA Lyon), and Université Grenoble Alpes (UGA). It is also financially supported by the Fond de Recherche du Québec Nature et Technologies FRQNT.

Appendix A. Supplementary data

Supplementary data to this article can be found online at https://doi.org/10.1016/j.bios.2022.114481.

References

Abadian, P.N., Kelley, C.P., Goluch, E.D., 2014. Cellular analysis and detection using surface plasmon resonance techniques. Anal. Chem. 86 (6), 2799–2812. https://doi.org/10.1021/ac500135s.

Aird, W.C., 2012. Endothelial cell heterogeneity. Cold Spring Harbor Perspectives in Medicine 2 (1). https://doi.org/10.1101/cshperspect.a006429 a006429–a006429.

Andrade-Gordon, P., Maryanoff, B.E., Derian, C.K., Zhang, H.-C., Addo, M.F., Darrow, A. L., Eckardt, A.J., Hoekstra, W.J., McComsey, D.F., Oksenberg, D., Reynolds, E.E., Santulli, R.J., Scarborough, R.M., Smith, C.E., White, K.B., 1999. Design, synthesis, and biological characterization of a peptide-mimetic antagonist for a tethered-ligand receptor. Proc. Natl. Acad. Sci. USA 96 (22), 12257–12262. https://doi.org/10.1073/pnas.96.22.12257.

Birdwell, C.R., Gospodarowicz, D., Nicolson, G.L., 1978. Identification, localization, and role of fibronectin in cultured bovine endothelial cells. Proc. Natl. Acad. Sci. USA 75 (7), 3273–3277. https://doi.org/10.1073/pnas.75.7.3273.

Bocková, M., Slabý, J., Špringer, T., Homola, J., 2019. Advances in surface plasmon resonance imaging and microscopy and their biological applications. Annu. Rev. Anal. Chem. 12 (1), 151–176. https://doi.org/10.1146/annurev-anchem-061318-115106.

Chabot, V., Cuerrier, C.M., Escher, E., Aimez, V., Grandbois, M., Charette, P.G., 2009. Biosensing based on surface plasmon resonance and living cells. Biosens. Bioelectron. 24 (6), 1667–1673. https://doi.org/10.1016/j.bios.2008.08.025.

Chen, C.S., Mrksich, M., Huang, S., Whitesides, G.M., Ingber, D.E., 1997. Geometric control of cell life and death. Science 276 (5317), 1425–1428. https://doi.org/10.1126/science.276.5317.1425.

Chen, C.S., Mrksich, M., Huang, S., Whitesides, G.M., Ingber, D.E., 1998. Micropatterned surfaces for control of cell shape, position, and function. Biotechnol. Prog. 14 (3), 356–363. https://doi.org/10.1021/bp980031m.

Cuerrier, C.M., Chabot, V., Vigneux, S., Aimez, V., Escher, E., Gobeil, F., Charette, P.G., Grandbois, M., 2008. Surface plasmon resonance monitoring of cell monolayer integrity: implication of signaling pathways involved in actin-driven morphological remodeling. Cell. Mol. Bioeng. 1 (4), 229–239. https://doi.org/10.1007/s12195-008-0028-4.

Dincer, C., Bruch, R., Costa-Rama, E., Fernández-Abedul, M.T., Merkoçi, A., Manz, A., Urban, G.A., Güder, F., 2019. Disposable sensors in diagnostics, food, and environmental monitoring. Adv. Mater. 1806739 https://doi.org/10.1002/adma.201806739.

Fang, Y., 2011. Label-free biosensors for cell biology. Int. J. Electrochem., 460850 https://doi.org/10.4061/2011/460850.

Gospodarowicz, D., Moran, J., Braun, D., Birdwell, C., 1976. Clonal growth of bovine vascular endothelial cells: fibroblast growth factor as a survival agent. Proc. Natl. Acad. Sci. USA 73 (11), 4120–4124. https://doi.org/10.1073/pnas.73.11.4120.

Gospodarowicz, D., Greenburg, G., Bialecki, H., Zetter, B.R., 1978. Factors involved in the modulation of cell proliferation in vivo and in vitro: the role of fibroblast and epidermal growth factors in the proliferative response of mammalian cells. In: In Vitro, vol. 14, pp. 85–118. https://doi.org/10.1007/BF02618177, 1.

Harris, C.R., Millman, K.J., Walt, S., van der, J., Gommers, R., Virtanen, P., Cournapeau, D., Wieser, E., Taylor, J., Berg, S., Smith, N.J., Kern, R., Picus, M., Hoyer, S., Kerkwijk, M., van, H., Brett, M., Haldane, A., R'ıo, J., del, F., Wiebe, M., Peterson, P., G'erard-Marchant, P., Sheppard, K., Reddy, T., Weckesser, W., Abbasi, H., Gohlke, C., Oliphant, T.E., 2020. Array programming with NumPy. Nature 585 (7825), 357–362. https://doi.org/10.1038/s41586-020-2649-2.

Huang, G., Li, F., Zhao, X., Ma, Y., Li, Y., Lin, M., Jin, G., Lu, T.J., Genin, G.M., Xu, F., 2017. Functional and biomimetic materials for engineering of the three-dimensional cell microenvironment. Chem. Rev. 117 (20), 12764–12850. https://doi.org/10.1021/acs.chemrev.7b00094.

Hunter, J., Matplotlib, D., 2007. A 2D graphics environment. Comput. Sci. Eng. 9 (3), 90–95. https://doi.org/10.1109/MCSE.2007.55.

Jeon, H., Simon, C.G., Kim, G., 2014. A mini-review: cell response to microscale, nanoscale, and hierarchical patterning of surface structure. J. Biomed. Mater. Res. B Appl. Biomater. 102 (7), 1580–1594. https://doi.org/10.1002/jbm.b.33158.

Kodoyianni, V., 2011. Label-free analysis of biomolecular interactions using SPR imaging. Biotechniques 50 (1), 32–40. https://doi.org/10.2144/000113569.

L'Heureux, N., Pâquet, S., Labbé, R., Germain, L., Auger, F.A., 1998. A completely biological tissue-engineered human blood vessel. Faseb. J. 12 (1), 47–56. https://doi.org/10.1096/fsb2fasebj.12.1.47.

Laposata, M., Dovnarsky, D., Shin, H., 1983. Thrombin-induced gap formation in confluent endothelial cell monolayers in vitro. Blood 62 (3), 549–556. https://doi.org/10.1182/blood.V62.3.549.549.

Legland, D., Arganda-Carreras, I., Andrey, P., MorphoLib, J., 2016. Integrated library and plugins for mathematical morphology with ImageJ. 3. Bioinformatics 32 (22), 3532–3534. https://doi.org/10.1093/bioinformatics/btw413.

Mehta, D., Malik, A.B., 2006. Signaling mechanisms regulating endothelial permeability. Physiol. Rev. 86 (1), 279–367. https://doi.org/10.1152/physrev.00012.2005.

Minami, T., Sugiyama, A., Wu, S.-Q., Abid, R., Kodama, T., Aird, W.C., 2004 Jan. Thrombin and phenotypic modulation of the endothelium. Arterioscler. Thromb. Vasc. Biol. 24 (1), 41–53. https://doi.org/10.1161/01.ATV.0000099880.09014.7D.

Mrksich, M., Whitesides, G.M., 1996. Using self-assembled monolayers to understand the interactions of man-made surfaces with proteins and cells. Annu. Rev. Biophys. Biomol. Struct. 25 (1), 55–78. https://doi.org/10.1146/annurev.bb.25.060196.000415.

Mrksich, M., Dike, L.E., Tien, J., Ingber, D.E., Whitesides, G.M., 1997. Using microcontact printing to pattern the attachment of mammalian cells to self-Exp. Cell Res. 235 (2), 305–313. https://doi.org/10.1006/excr.1997.3668.

Nobe, K., Sone, T., Paul, R.J., Honda, K., 2005. Thrombin-induced force development in vascular endothelial cells: contribution to alteration of permeability mediated by calcium-dependent and -independent pathways. J. Pharmacol. Sci. 99 (3), 252–263. https://doi.org/10.1254/jphs.FP0050679.

Opal, S.M., van der Poll, T., 2015. Endothelial barrier dysfunction in septic shock. J. Intern. Med. 277 (3), 277–293. https://doi.org/10.1111/joim.12331.

Parker, K.K., Brock, A.L., Brangwynne, C., Mannix, R.J., Wang, N., Ostuni, E., Geisse, N. A., Adams, J.C., Whitesides, G.M., Ingber, D.E., 2002. Directional control of lamellipodia extension by constraining cell shape and orienting cell tractional forces. Faseb. J. 16 (10), 1195–1204. https://doi.org/10.1096/fj.02-0038com.

Pedregosa, F., Varoquaux, G., Gramfort, A., Michel, V., Thirion, B., Grisel, O., Blondel, M., Prettenhofer, P., Weiss, R., Dubourg, V., Vanderplas, J., Passos, A., Cournapeau, D., Brucher, M., Perrot, M., Duchesnay, E., 2011. Scikit-learn: machine learning in Python. J. Mach. Learn. Res. 12, 2825–2830.

Reglero-Real, N., Colom, B., Bodkin, J.V., Nourshargh, S., 2016. Endothelial cell junctional adhesion molecules: role and regulation of expression in inflammation. Arterioscler. Thromb. Vasc. Biol. 36 (10), 2048–2057. https://doi.org/10.1161/ATVBAHA.116.307610.

Söllradl, T., Banville, F.A., Chabot, V., Canva, M., Grandbois, M., Charette, P.G., 2017. Metal clad waveguide (MCWG) based imaging using a high numerical aperture microscope objective. Opt. Express, OE 25 (3), 1666–1679. https://doi.org/10.1364/OE.25.001666.

Söllradl, T., Chabot, K., Fröhlich, U., Canva, M., Charette, P.G., Grandbois, M., 2018a. Monitoring individual cell-signaling activity using combined metal-clad waveguide and surface-enhanced fluorescence imaging. Analyst 143 (22), 5559–5567. https://doi.org/10.1039/C8AN00911B.

Söllradl, T., Banville, F.A., Fröhlich, U., Canva, M., Charette, P.G., Grandbois, M., 2018b. Label-free visualization and quantification of single cell signaling activity using metal-clad waveguide (MCWG)-Based microscopy. Biosens. Bioelectron. 100 (Suppl. C), 429–436. https://doi.org/10.1016/j.bios.2017.09.002.

Shchukarev, A., Korolkov, D., 2004. XPS study of group IA carbonates. Open Chemistry 2 (2), 347–362. https://doi.org/10.2478/BF02475578.

Théry, M., 2010. Micropatterning as a tool to decipher cell morphogenesis and functions. J. Cell Sci. 123 (24), 4201–4213. https://doi.org/10.1242/jcs.075150.

Théry, M., Racine, V., Pépin, A., Piel, M., Chen, Y., Sibarita, J.-B., Bornens, M., 2005. The extracellular matrix guides the orientation of the cell division Axis. Nat. Cell Biol. 7 (10), 947–953. https://doi.org/10.1038/ncb1307.

Théry, M., Pépin, A., Dressaire, E., Chen, Y., Bornens, M., 2006. Cell distribution of stress fibres in response to the geometry of the adhesive environment. Cell Motil Cytoskeleton 63 (6), 341–355. https://doi.org/10.1002/cm.20126.

Toomre, D., Bewersdorf, J., 2010. A new wave of cellular imaging. Annu. Rev. Cell Dev. Biol. 26 (1), 285–314. https://doi.org/10.1146/annurev-cellbio-100109-104048.

Tseng, Q., Duchemin-Pelletier, E., Deshiere, A., Balland, M., Guillou, H., Filhol, O., Thery, M., 2012. Spatial organization of the extracellular matrix regulates cell-cell junction positioning. Proc. Natl. Acad. Sci. USA 109 (5), 1506–1511. https://doi.org/10.1073/pnas.1106377109.

Ulman, A., 1996. Formation and structure of self-assembled monolayers. Chem. Rev. 96 (4), 1533–1554. https://doi.org/10.1021/cr9502357.

Van der Walt, S., Schönberger, J.L., Nunez-Iglesias, J., Boulogne, F., Warner, J.D., Yager, N., Gouillart, E., Yu, T., 2014. contributors, the scikit-image. Scikit-Image: image Processing in Python. PeerJ 2, e453. https://doi.org/10.7717/peerj.453.

Van Hinsbergh, V.W.M., 2001. The endothelium: vascular control of haemostasis. Eur. J. Obstet. Gynecol. Reprod. Biol. 95 (2), 198–201. https://doi.org/10.1016/S0301-2115(00)00490-5.

Vandenbroucke, E., Mehta, D., Minshall, R., Malik, A.B., 2008. Regulation of endothelial junctional permeability. Ann. N. Y. Acad. Sci. 1123 (1), 134–145. https://doi.org/10.1196/annals.1420.016.

Versaevel, M., Grevesse, T., Gabriele, S., 2012. Spatial coordination between cell and nuclear shape within micropatterned endothelial cells. Nat. Commun. 3 (1), 671. https://doi.org/10.1038/ncomms1668.

Vlodavsky, I., JOHNSONt, L.K., Gospodarowicz, D., 1979. Appearance in confluent vascular endothelial cell monolayers of a specific cell surface protein (CSP-60) not detected in actively growing endothelial cells or in cell types growing in multiple layers. Cell Biol. 76 (5), 2306–2310. https://doi.org/10.1073/pnas.76.5.2306.

Vouret-Craviari, V., Boquet, P., Pouysségur, J., Van Obberghen-Schilling, E., 1998. Regulation of the actin cytoskeleton by thrombin in human endothelial cells: role of rho proteins in endothelial barrier function. MBoC 9 (9), 2639–2653. https://doi.org/10.1091/mbc.9.9.2639.

Wallez, Y., Huber, P., 2008. Endothelial adherens and tight junctions in vascular homeostasis, inflammation and angiogenesis. Biochim. Biophys. Acta Biomembr. 1778 (3), 794–809. https://doi.org/10.1016/j.bbamem.2007.09.003.

We Help You Make Masks. (*www.photomaskportal.com*).

Yanase, Y., Hiragun, T., Ishii, K., Kawaguchi, T., Yanase, T., Kawai, M., Sakamoto, K., Hide, M., 2014. Surface plasmon resonance for cell-based clinical diagnosis. Sensors 14 (3), 4948–4959. https://doi.org/10.3390/s140304948.

Zaidel-Bar, R., Itzkovitz, S., Ma'ayan, A., Iyengar, R., Geiger, B., 2007. Functional atlas of the integrin adhesome. Nat. Cell Biol. 9 (8), 858–867. https://doi.org/10.1038/ncb0807-858.

Zania, P., Kritikou, S., Flordellis, C.S., Maragoudakis, M.E., Tsopanoglou, N.E., 2006. Blockade of angiogenesis by small molecule antagonists to protease-activated receptor-1: association with endothelial cell growth suppression and induction of apoptosis. J. Pharmacol. Exp. Therapeut. 318 (1), 246–254. https://doi.org/10.1124/jpet.105.099069.